RSC Advances

PAPER

View Article Online
View Journal | View Issue

Cite this: *RSC Adv.*, 2024, **14**, 15656

Catalytic performance of modified carbon black on methane decomposition for hydrogen production

Niuhu Zhou,[ab] Donglin Zhao,[ab] Qin Su,[ab] Qiongguang Li,[ab] Weiwei Zha[ab] and Shaojie Feng *[ab]

Carbon-based catalysts catalyze methane decomposition to produce hydrogen is a very attractive technical route. Carbon black in carbon-based catalysts has the advantages of high catalytic activity, good stability and better tolerance to toxic impurities such as sulphur in the feedstock, which has become a hot topic of research for many scientists. In this work, the effect of heat treatment on the structural and surface properties of carbon blacks and their catalytic performance in hydrogen production from methane decomposition was investigated. A commercial carbon blacks N110 was selected to heat treatment with nitrogen or carbon dioxide atmosphere at 850 °C, respectively. The Raman spectrums indicated that the graphitization degree of modified carbon under two atmospheres were promoted with the treatment time increasing. BET results revealed that the specific surface area of the carbon black treated under carbon dioxide increased, while the specific surface area was unchanged for that of the carbon black treated under nitrogen. The catalytic test of the two modified carbon blacks for methane decomposition exhibited the almost same activity, which meant that the graphitization degree of carbon black is the key factor for methane decomposition rather than the specific surface area. It was suggested that highly graphitized carbon black could be used as the potential catalysts for hydrogen production from methane decomposition.

Received 26th February 2024
Accepted 23rd April 2024

DOI: 10.1039/d4ra01486c

rsc.li/rsc-advances

1. Introduction

In recent years, the intensive burning of fossil fuels has caused serious environmental pollution and global warming.[1] Adopting low-carbon energy has become a global consensus. As a clean energy source, hydrogen is not only used as a high-energy fuel, widely used in the aerospace industry such as rockets and space shuttles. It's also widely used in many fields such as oil refining, metallurgy and the food industry.[2,3]

Currently, the main processes for hydrogen production are: steam methane (SMR)/dry reforming (DRM), catalytic methane decomposition (CMD), partial oxidation of methane (POM), water decomposition and coal/biomass gasification. Water decomposition processes driven by electricity or light to produce H_2 are extremely interesting to study and there are no CO_2 emissions during the production of H_2.[4] However, for light-driven water decomposition experiment, yields and costs are still extremely challenging for practical applications. SMR and DRM are the dominant hydrogen production processes today. Despite their maturity, these processes inevitably produce CO or CO_2 by-products.[5] Furthermore, complex and expensive separation processes are required to remove CO_x from the hydrogen stream. Hydrogen production from biomass gasification using various biomass sources (*e.g.*, forest residues, wood waste, microalgae, crop residues and waste cooking oil) is also associated with large amounts of carbon dioxide, which has a significant impact on global warming. In contrast to these processes, CMD is a promising and environmentally friendly technology for hydrogen production. It is a heat-absorbing process with solid carbon and gaseous hydrogen as products. The reaction equation is as follows:

$$CH_4(g) \rightarrow C(s) + 2H_2(g),\ \Delta H = 75.6\ \text{kJ mol}^{-1}$$

Metal-based catalysts are commonly used for methane decomposition. The Fe,[6–8] Co,[9,10] Ni,[11–13] Cu,[14,15] *etc.* metal catalysts were reported to catalyze methane decomposition. Metal-based catalysts typically have high catalytic activity and low reaction temperatures. However, carbon deposits on the surface of metal catalysts, which cause the catalyst to deactivate, limited their application.

Carbon materials (activated carbon AC,[16,17] CMK,[18,19] coal char,[20,21] carbon black,[22–24] *etc.*) are also commonly used in the catalytic decomposition of methane to produce hydrogen. Carbon materials can accommodate more carbon deposition in the CMD process than metal catalysts, mainly due to their high

[a]Key Laboratory of Functional Molecule Design and Interface Process, Anhui Jianzhu University, Hefei, 230601, China. E-mail: fengshaojie@ahjzu.edu.cn
[b]Anhui Province International Center on Advanced Building Materials, Anhui Jianzhu University, Hefei, 230601, China

specific surface area and abundant pore space. Carbon materials have better tolerance and conversion stability to sulfur and other toxic impurities in the feedstock, although they perform less well in CMD. The hydrogen production rate of carbon materials with different structures varies widely. It was reported that carbon black has the highest hydrogen production rate from methane decomposition of all carbon catalysts.[4,25] However, it is not clear whether the structure or the surface area of the carbon material plays the key role in the catalytic decomposition of methane.

In this work, we aim to prepare modified carbon blacks with different structures by modulating the carbon black structure through heat treatment methods. The effect of heat treatment time on the structure and catalytic performance of the catalysts was investigated, and it was also explored whether the key factor affecting the catalytic performance was the graphitization degree or the specific surface area of the carbon black.

2. Experimental

2.1 Materials preparation

The commercial carbon black N110 (Anhui Black Cat New Materials Co., Ltd.) was selected as carbon precursor. The N110 was ground and sieved to 40–60 mesh and then oxidized in a tube furnace at 850 °C under CO_2 or N_2 atmosphere for different time. The commercial carbon black is marked as N110. Carbon material treated at 850 °C for two hours under N_2 atmosphere is marked as CB-N_2-2. Carbon material treated at 850 °C for different time under CO_2 atmosphere is marked as CB-CO_2-X (X = 1 h, 2 h, 3 h, 4 h).

2.2 Characterization

The crystal structure of carbon materials was analyzed by X-ray diffractometer (Bruker D8 ADVANCE) with Cu Kα radiation (λ = 1.5406 Å). High-resolution field emission scanning electron microscopy (Regulus 8230, Hitachi, Japan) were used to study the morphologies and elemental compositions of the samples. A physical adsorption analyzer (ASAP 2460, Micromeritics, USA) was used to measure the surface area (BET) and pore size distribution of the catalyst by nitrogen (N_2) adsorption at −195.85 °C. Structures of carbon materials were analyzed by Raman spectroscopy (Thermo Fisher Dxr2xi). X-ray photoelectron spectroscopy (EscaLab QXi) was used to determine the elemental composition of the catalyst surface.

2.3 Catalytic decomposition of methane

Catalytic decomposition of methane (CMD) was carried out in a fixed-bed quartz reactor with an inner diameter of 6 mm at atmospheric pressure. 0.2 g of catalyst was placed in the center of the reactor and heated to 850 °C with 33 mL min^{-1} nitrogen flow. And then, nitrogen flow was switched to the methane gas with 33 mL min^{-1}. The total gas hourly space velocity (GHSV) was set at 10 000 mL (h^{-1} g_{cat}^{-1}). After ten minutes of reaction, the composition of the gas products was analyzed by a gas chromatograph (GC-14C). Methane conversion and hydrogen yield were calculated by the following equations:

$$X_{CH_4} = (F_{CH_4;in} - F_{CH_4;out})/F_{CH_4;in} \times 100\%$$

$$Y_{H_2;out} = 2(F_{CH_4;in} - F_{CH_4;out})/m$$

where X, Y, F, and m denote the conversion of CH_4 (%), hydrogen yield (mmol (g^{-1} min^{-1})), gas flow rate (mmol min^{-1}), and catalyst mass (g), respectively.

3. Results

3.1 Effect of heat treatment on the properties of carbon black

Fig. 1 shows the XRD patterns of carbon materials for N110, CB-N_2-2 and CB-CO_2-X (X = 1, 2, 3, 4 h). Two characteristic carbon diffraction peaks at 26° and 43°, corresponding to the C(002) and C(101) lattice planes, are observed in all carbon materials (a–f). It's clearly indicated that all of the carbon materials show a kind of graphitic-like structure.[31] The intensity ratios $I_C(101)/I_C(002)$ indicate the order of the graphene sheets in the carbon material. The lower the ratio, the higher the order of the structure. The higher ratio means the lower order of the structure. As can be seen in Fig. 1, the $I_C(101)/I_C(002)$ ratios of the treated carbon materials (b, c, d, e and f) are lower than N110 (a), which suggests that the heat-treated carbon is more order than N110. For the two modified carbon blacks treated at same time under different atmospheric environments (N_2 or CO_2), it found that the $I_C(101)/I_C(002)$ ratios of CB-N_2 (b) and CB-CO_2-2 (d) are almost constant. However, under the same atmosphere environment (CO_2) and with different treatment times, it is found that the order of the carbon material is increased with the increase of heat treatment time. The results indicates that the treatment time has an effect on the structural order of carbon materials, but the treatment atmosphere has no effect on the order of the carbon material lattice.

Fig. 2 shows the specific surface area (Fig. 2a) and total pore volume (Fig. 2b) of N110, CB-N_2-2 and CB-CO_2-X (X = 1, 2, 3, 4);

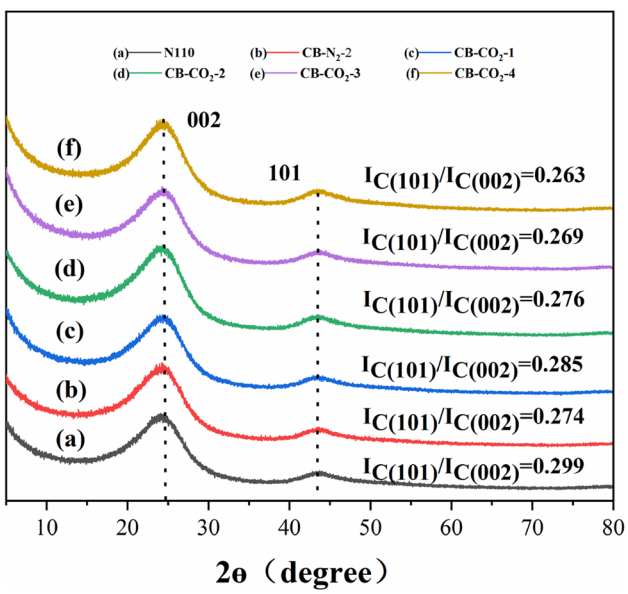

Fig. 1 XRD of N110 (a), CB-N_2-2 (b) and CB-CO_2-X (X = 1, 2, 3, 4 h) (c–f).

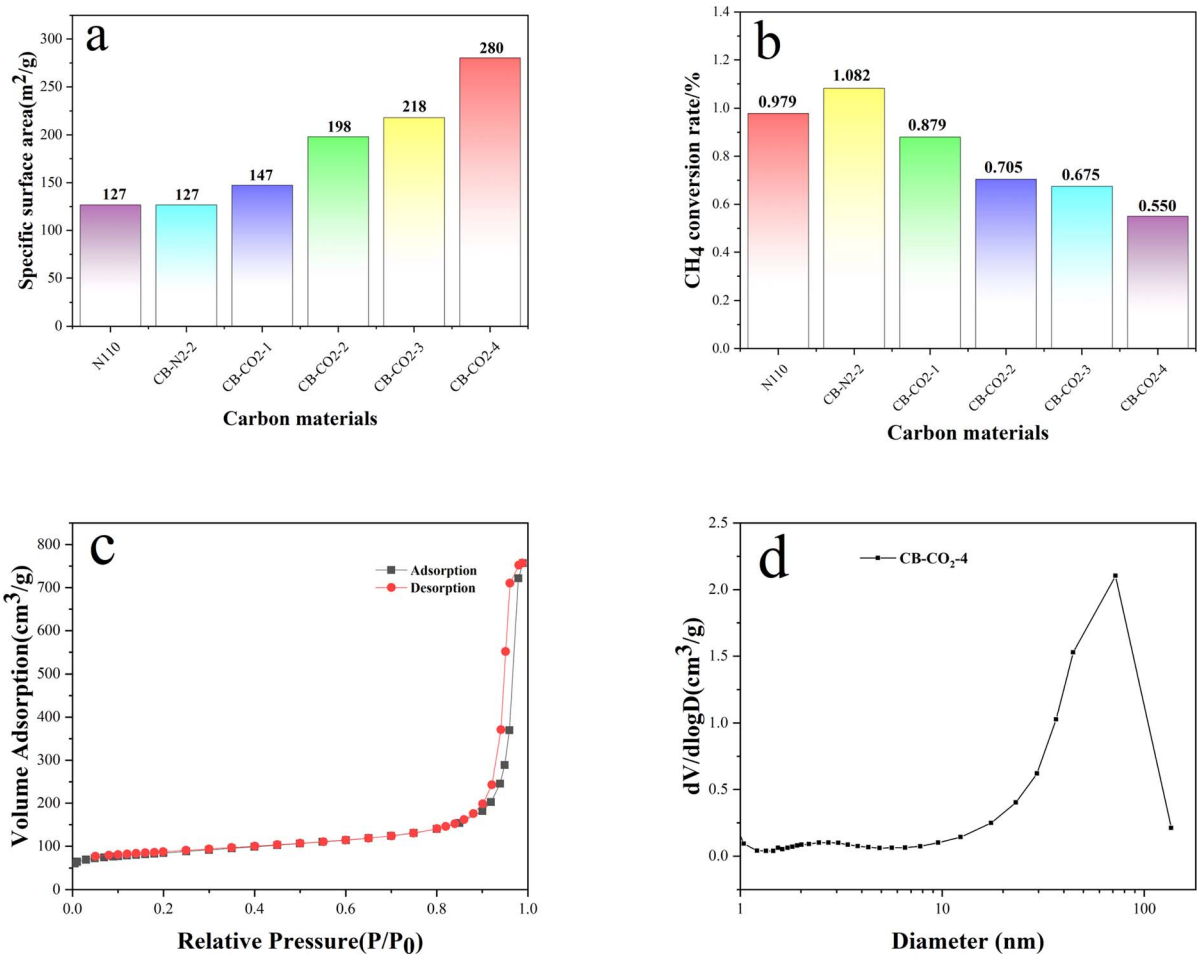

Fig. 2 Specific surface area (a) and total pore volume (b) of N110, CB-N_2-2 and CB-CO_2-X (X = 1, 2, 3, 4); isotherms (c) and pore size distributions (d) of CB-CO_2-4 (X = 1, 2, 3, 4).

isotherms (Fig. 2c) and pore size distribution (Fig. 2d) of CB-CO_2-4 (X = 1, 2, 3, 4). Fig. 2a clearly shows that the specific surface area of carbon black increased after high temperature treatment with carbon dioxide. Comparing with Fig. 2b, it is found that the results are almost the same as Fig. 2a, the pore volume of carbon black increases with the increase of carbon dioxide treatment time. Fig. 2c and d show the adsorption isotherm and pore size distribution of CB-CO_2-4, respectively. In Fig. 2c, it was found that the CB-CO_2-4 sample exhibited a type IV isotherm. For the type IV isotherm, hysteresis occurs in the desorption stage to the extent that capillary condensation occurs due to capillary condensation on the pores or irregular surfaces during the adsorption process. The average particle size of the CB-CO_2-4 sample is 72 nm with a macroporous nature as can be observed in Fig. 2d. The main reason for the larger specific surface area of the CB-CO_2-4 sample may be due to the redox reaction of carbon black in a carbon dioxide atmosphere, where carbon dioxide streams are flushed from the surface of the carbon black to form macropores.[26]

Fig. 3 shows the SEM images of N110 (a), CB-N_2-2 (b) and CB-CO_2-4 (c). As can be seen in Fig. 3a, the surface of N110 is relatively rough and well-defined, the particle size is about 30 nm, and the particles are adsorbed with each other to form large agglomerates. Fig. 3b shows that N110 was treated at high temperatures with a large range of sintering of the carbon particles and the formation of large pores. It is clear from Fig. 3c that the high temperature treatment in a carbon dioxide atmosphere makes the pores richer. At the same time, many pores appeared on the carbon surface in the presence of carbon dioxide gas flow. This is consistent with the BET results, which are mainly related to the oxidation reaction of the carbon material.

The XPS spectra of N110 and CB-CO_2-4 are shown in Fig. 4. Fig. 4a shows the carbon spectrum on the N110 surface and Fig. 4b shows the carbon spectrum on the CB-CO_2-4 surface. According to the C 1s precision spectral analysis, N110 consists of four main spectral peaks, and there are four positional binding energies on the surfaces of N110 and CB-CO_2-4, 284.8 eV, 286.2 eV, 287.5 eV, and 289.9 eV, which correspond to the carbon compositions of C–C/C–H (adsorbed carbon), C–O, C═O, and carbonate, respectively. N110 and CB-CO_2-4 surfaces are dominated by sp^3 C–C. The rest of the peaks represent the C–O, C═O and carbonate chemical states of the carbon materials, respectively. Comparison of the C 1s spectra of N110 and CB-CO_2-4 shows that the C–O and C═O compositions are quite different. It may be due to reduction of C–O and C═O by redox

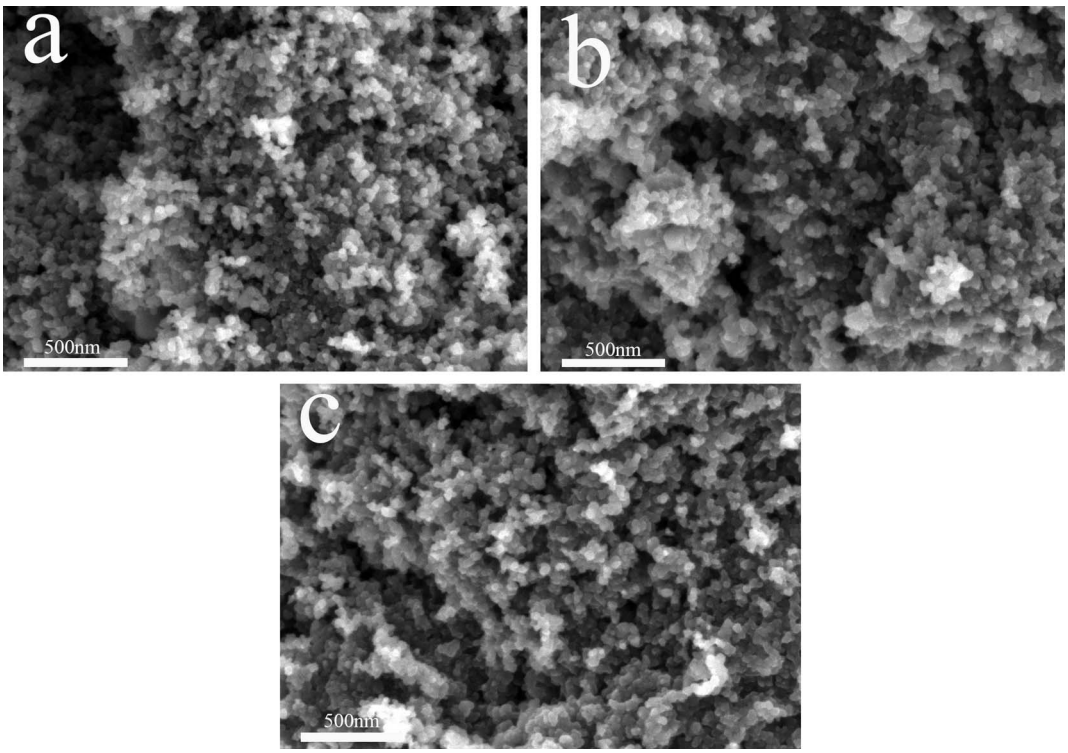

Fig. 3 SEM of N110 (a), CB-N_2-2 (b) and CB-CO_2-4 (c).

reaction of surface oxides with C during high temperature treatment of N110.

3.2 Catalytic methane decomposition of modified carbon blacks

Fig. 5a shows the initial catalytic performance of N110, CB-N_2-2 and CB-CO_2-X (X = 1, 2, 3, 4 h) catalyzing the methane decomposition reaction. No C_2 hydrocarbon products were detected in the effluent, which means 100% hydrogen selectivity. The methane conversion and hydrogen production rates varied with increasing graphitization degree of the carbon material. As can be seen in Fig. 5a, the highest initial methane conversion of 15.4% was achieved after treating the carbon with CO_2 at high temperature for 4 hours. Compared with the initial methane conversion of 12.4% for the N110, the catalytic performance was improved by 23.9%.

In recent years, it is controversial whether the specific surface area or the graphitization degree of carbon materials affects the catalytic performance of methane.[20,25,27] The initial methane conversion and hydrogen production rates of all treated carbon materials (CB-N_2-2 and CB-CO_2-X) are significantly higher than those of N110, which indicates that the heat-treated carbon is more favorable for methane catalytic

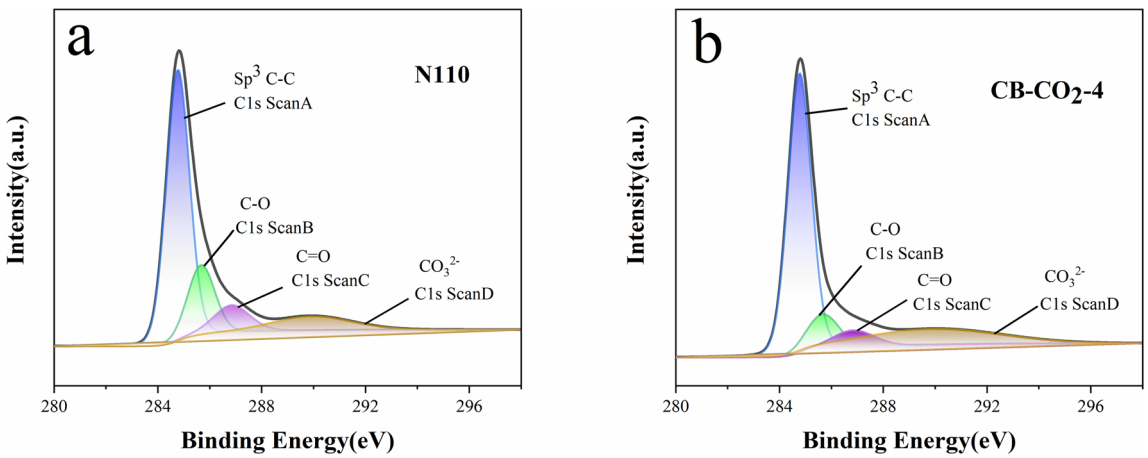

Fig. 4 C 1s XPS for N110 (a) and CB-CO_2-4 (b).

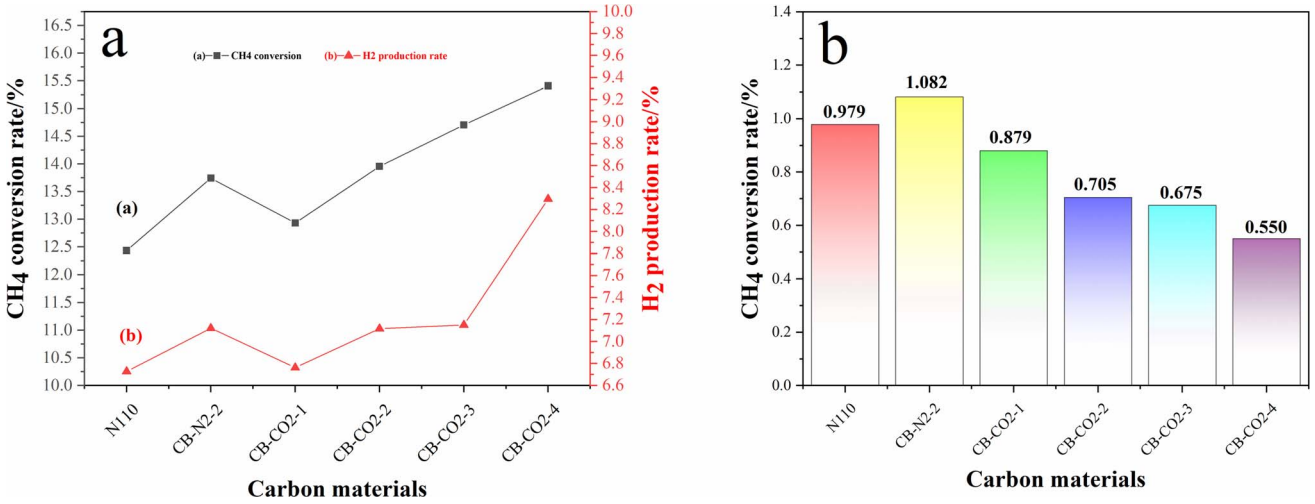

Fig. 5 Initial methane activity diagram (a) and the methane conversion rate per unit specific surface area (b).

decomposition than that of N110. The specific surface area of the carbon material treated in the carbon dioxide atmosphere was much larger than that of the carbon material treated in the nitrogen atmosphere for the same treatment time, but the methane conversion was almost the same for both. Furthermore, the methane conversion over the modified carbon blacks was increased with the extension of heat treatment time under the same atmosphere environment (CO_2) and different treatment time. The results suggest that the prolonging the heat treatment time of carbon materials is beneficial to the catalytic properties of carbon black, but the type of treatment atmosphere had no effect on the catalytic decomposition of methane. Therefore, we investigated the methane conversion per unit mole of carbon material to see if the specific surface area was a crucial factor in the catalytic performance of methane.

Fig. 5b shows the methane conversion per unit specific surface area of carbon materials. It clearly shows that the methane conversion per unit specific surface area decreases with increasing oxidation treatment time in a carbon dioxide atmosphere. Comparing Fig. 5b with Fig. 2a, it can be seen that the specific surface areas of N110 and CB-N_2-2 are the same, while the methane conversion per unit specific surface area is different. The results indicate that the specific surface area of the carbon materials is not a factor affecting the catalytic performance of methane. This result contradicts the findings of Muradov *et al.*[25]

Fig. 6 shows the XRD spectra of N110 (a), CB-N_2-2 (c), CB-CO_2-4 (e) before catalysis and N110 (b), CB-N_2-2 (d), CB-CO_2-4 (f) after catalysis. Fig. 6 shows visually that the $I_C(101)/I_C(002)$ ratios of catalysts (a), (c), and (e) are decreased compared to those of catalysts (b), (d), and (f), respectively. The result indicates that the carbon material catalysts are more ordered after catalysis than before catalysis, which means that the catalytic decomposition of methane is a process of ordered carbon deposition.

In order to have a more in-depth observation of the carbon deposits produced on the catalyst surface, SEM images of used N110 (Fig. 7a), used CB-N_2-2 (Fig. 7b), and used CB-CO_2-4 (Fig. 7c) were compared with Fig. 3. It was found that the catalyzed carbon grains intersected, grew and aggregated with each other. The produced carbon grew and deposited on the surface of the original carbon material.

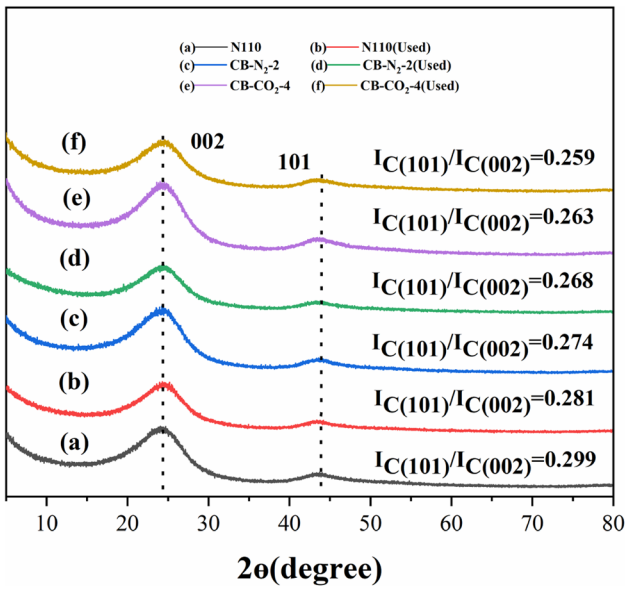

Fig. 6 XRD of N110 (a), CB-N_2-2 (c), CB-CO_2-4 (e) and used N110 (b), used CB-N_2-2 (d), used CB-CO_2-4 (f).

4. Discussion

In this work, we prepared highly graphitized carbon materials by heat treatment. The heat treatment process also increased the graphite lattice defects. The graphite lattice defects are **FRONT**, **FISSURE**, **BAY**, **COVE** and **FJORD**, and the main structures of these graphite lattice defects are shown in Fig. 8. The **BAY** clusters are more active than the **FISSURE** clusters because the **BAY** clusters require two carbon atoms to form a hexagonal

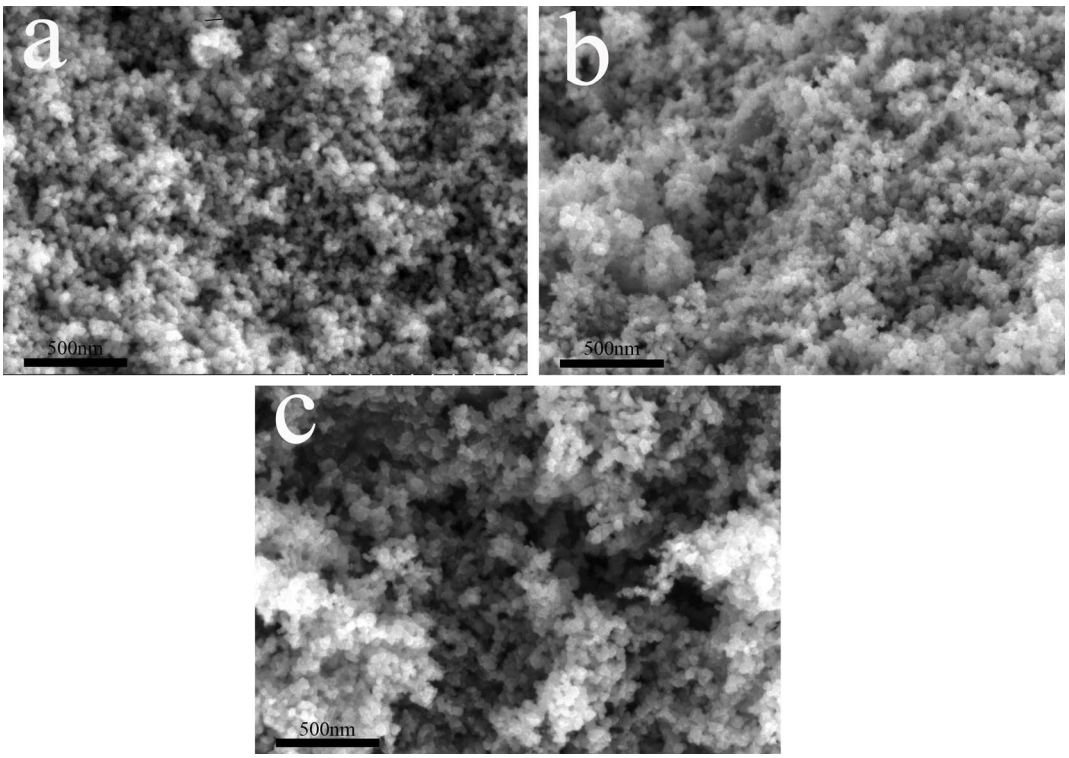

Fig. 7 SEM of used N110 (a), used CB-N_2-2 (b) and used CB-CO_2-4 (c).

ring, while the **FISSURE** clusters require three carbon atoms.[28] In addition, there is strong D-band scattering in the **BAY** cluster, in contrast to the **FISSURE** cluster where D-band scattering is forbidden. The I_D/I_G of each catalyst is thus intimately linked to its catalytic activity.

The surface properties of the treated carbon black was investigated by Raman characterization. Fig. 9 shows the Raman spectra of the carbon materials. All the samples showed absorption peaks at 1345 cm^{-1} and 1595 cm^{-1}, which correspond to the D and G peaks of carbon materials, respectively.[29] The D peak is believed to be caused by structural defects in the graphite layer, while the G peak is caused by the expansion and contraction vibrations of the sp^2 hybridized carbon atoms in the 2D hexagonal lattice. It is well known that the intensity ratio ($I_D : I_G$) of the D and G peaks indicates the graphitization degree of carbon materials. This means that the smaller the $I_D : I_G$ ratio, the higher the graphitization degree. Fig. 9a clearly shows that the I_D/I_G ratios of the treated carbon materials (b–f) are lower than those of N110, indicating that the heat treated carbon materials have a higher graphitization degree than N110. The I_D/I_G ratios of CB-N_2-2 (b) and CB-CO_2-2 (d) were found to be almost the same for commercial carbon black N110 treated at high temperature for the same time under N_2 and CO_2 atmospheres, respectively. However, it was found that the graphitization degree of the modified carbon materials (c, d, e and f) was increased with the increase of heat treatment time under the same atmosphere environment (CO_2). The result indicates that the treatment time is the key factor in increasing the graphitization degree of carbon materials rather than the treatment atmosphere. This result agrees with the XRD results that the more graphitized of the carbon material correspond to the more order of structure.

Fig. 9b shows the Raman spectra of N110 (a), CB-N_2-2 (c), CB-CO_2-4 (e) before catalysis and N110 (b), CB-N_2-2 (d), CB-CO_2-4 (f) after catalysis. The $I_D : I_G$ ratios of the post-catalyzed carbon materials are all larger than that of the pre-catalyzed

Fig. 8 Structure of five graphite lattice defects.

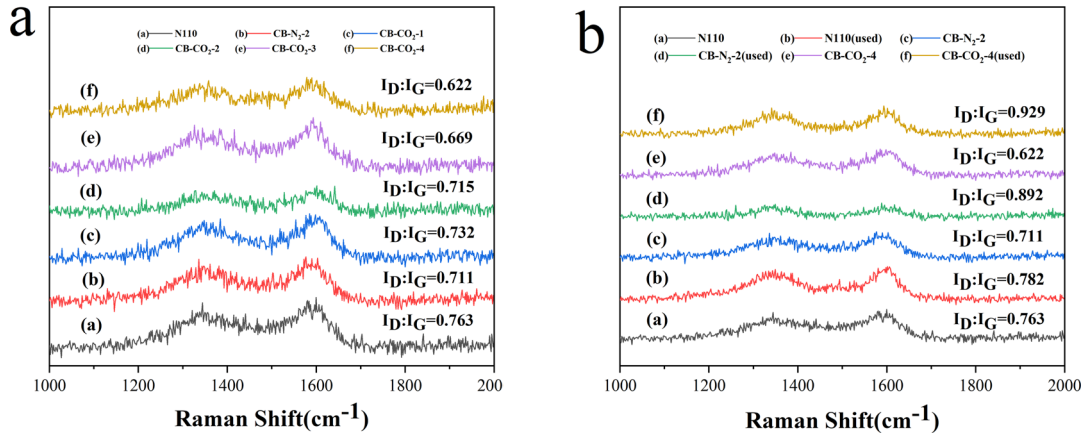

Fig. 9 Raman spectra of carbon materials before catalysis (a) and before and after comparative catalysis (b).

ones, and the D peak defects are also increased after catalysis. Combined with the catalytic performance graph (Fig. 5) and Raman spectra (Fig. 9), it was found that the catalytic performance increased as the graphitization degree increased. The catalytic results proved that the high graphitization carbon materials promoted the decomposition of methane. Comparison of the BET data and catalytic performance of two carbon materials (CB-N_2-2 and CB-CO_2-2) showed that the catalytic performance was almost constant for carbon materials with different specific surface areas, which suggests that the graphitization degree of the carbon materials plays a key role in methane decomposition rather than the specific surface area. The result is consistent with related reports that the active site for the decomposition of methane is located in the vicinity of the graphite edge.[30]

The higher I_D/I_G ratio of N110 than other catalysts may be related to the low methane conversion. In addition, the I_D/I_G ratio of CB-CO_2-4 before catalysis is 0.622, which is lower than that of CB-N_2-2 and N110. The result indicates that the defect density on the CB-CO_2-4 surface is higher than that on N110 and CB-N_2-2, or that many **BAY** clusters are distributed in the graphite edges of the CB-CO_2-4 surface. The initial methane conversion of CB-N_2-2 is almost the same as that of CB-CO_2-2, even though the specific surface area of CB-N_2-2 is lower than that of CB-CO_2-2. The combination of XRD and Raman patterns showed that high temperature heat treatment can change the structure of carbon materials, increase the graphitization degree, increase the structural order of carbon black and at the same time increase the degree of graphite defects. The catalytic results confirm that the higher the graphitization degree and the more ordered the structure of the carbon black, the better the catalytic performance. The experimental results also showed that the graphitization degree of carbon materials is a key factor affecting the catalytic performance of methane.

5. Conclusion

Modified carbon blacks with different graphitization degrees and different surface areas were prepared by high temperature heat treatment using carbon dioxide and nitrogen. The modified carbon CB-CO_2-4 showed better catalytic activity compared to N110. The initial methane conversion of CB-CO_2-4 reached 15.4%, which is a 23.9% increase in catalytic performance compared to 12.4% for N110. The experimental results show that high temperature heat treatment can modify the structure of carbon materials and increase the graphitization degree, while increasing the degree of graphite defects. Also, the results proved that the graphitization degree of carbon materials is a key factor affecting the catalytic performance of methane. This work provided a new way to modulate the structure of carbon materials, which has a wide range of potential applications in carbon materials catalyzing hydrogen production from methane decomposition.

Conflicts of interest

The authors declare that they have no known competing financial interests or personal relationships that could have appeared to influence the work reported in this paper.

Acknowledgements

This work was supported by the Science and Technology Major Special Project of Anhui Province (201903a07020002) and the Key Research and Development Project of Anhui Province (201904b11020041).

References

1 I. R. Hamdani and A. N. Bhaskarwar, Cu_2O nanowires based p-n homojunction photocathode for improved current density and hydrogen generation through solar-water splitting, *Int. J. Hydrogen Energy*, 2021, **46**, 28064–28077.
2 M. Simonov, Y. Bespalko, E. Smal, K. Valeev, V. Fedorova, T. Krieger and V. Sadykov, Nickel-containing ceria-zirconia doped with Ti and Nb. effect of support composition and preparation method on catalytic activity in methane dry reforming, *Nanomaterials*, 2020, **10**, 1281.
3 I. R. Hamdani and A. N. Bhaskarwar, Tuning of the structural, morphological, optoelectronic and interfacial

properties of electrodeposited Cu_2O towards solar water-splitting by varying the deposition pH, *Sol. Energy Mater. Sol. Cells*, 2022, **240**, 111719.

4 S. H. Hong, S. H. Ahn, J. Choi, *et al.*, High-activity electrodeposited NiW catalysts for hydrogen evolution in alkaline water electrolysis, *Appl. Surf. Sci.*, 2015, **349**, 629–635.

5 N. Muradov, Catalysis of methane decomposition over elemental carbon, *Catal. Commun.*, 2001, **2**, 89–94.

6 L. Zhou, L. R. Enakonda, Y. Saih, S. Loptain, D. Gary, P. Del-Gallo and J. M. Basset, Catalytic methane decomposition over Fe-Al_2O_3, *ChemSusChem*, 2016, **9**, 1243–1248.

7 L. Tang, D. Yamaguchi, N. Burke, D. Trimm and K. Chiang, Methane decomposition over ceria modified iron catalysts, *Catal. Commun.*, 2010, **11**, 1215–1219.

8 I.-W. Wang, D. A. Kutteri, B. Gao, H. Tian and J. Hu, Methane pyrolysis for carbon nanotubes and COx-free H_2 over transition-metal catalysts, *Energy Fuels*, 2018, **33**, 197–205.

9 S. Takenaka, M. Ishida, M. Serizawa, E. Tanabe and K. Otsuka, Formation of carbon nanofibers and carbon nanotubes through methane decomposition over supported cobalt catalysts, *J. Phys. Chem. B*, 2004, **108**, 11464–11472.

10 S.-P. Chai, S. H. S. Zein and A. R. Mohamed, Preparation of carbon nanotubes over cobalt-containing catalysts via catalytic decomposition of methane, *Chem. Phys. Lett.*, 2006, **426**, 345–350.

11 M. Ermakova, D. Y. Ermakov, G. Kuvshinov and L. Plyasova, New nickel catalysts for the formation of filamentous carbon in the reaction of methane decomposition, *J. Catal.*, 1999, **187**, 77–84.

12 J. Ziebro, I. Łukasiewicz, E. Borowiak-Palen and B. Michalkiewicz, Low temperature growth of carbon nanotubes from methane catalytic decomposition over nickel supported on a zeolite, *Nanotechnology*, 2010, **21**, 145308.

13 F. S. Al-Mubaddel, R. Kumar, M. L. Sofiu, F. Frusteri, A. A. Ibrahim, V. K. Srivastava, S. O. Kasim, A. H. Fakeeha, A. E. Abasaeed and A. I. Osman, Optimizing acido-basic profile of support in Ni supported La_2O_3 + Al_2O_3 catalyst for dry reforming of methane, *Int. J. Hydrogen Energy*, 2021, **46**, 14225–14235.

14 P. Ammendola, R. Chirone, L. Lisi, G. Ruoppolo and G. Russo, Copper catalysts for H_2 production via CH_4 decomposition, *J. Mol. Catal. A: Chem.*, 2007, **266**, 31–39.

15 T. V. Reshetenko, L. B. Avdeeva, Z. R. Ismagilov, A. L. Chuvilin and V. A. Ushakov, Carbon capacious Ni-Cu-Al_2O_3 catalysts for high-temperature methane decomposition, *Appl. Catal., A*, 2003, **247**, 51–63.

16 M. Szymańska, A. Malaika, P. Rechnia, A. Miklaszewska and M. Kozłowski, Metal/activated carbon systems as catalysts of methane decomposition reaction, *Catal. Today*, 2015, **249**, 94–102.

17 Z. Bai, H. Chen, B. Li and W. Li, Methane decomposition over Ni loaded activated carbon for hydrogen production and the formation of filamentous carbon, *Int. J. Hydrogen Energy*, 2007, **32**, 32–37.

18 R. Ryoo, S. H. Joo, S. Jun, T. Tsubakiyama and O. Terasaki, Ordered mesoporous carbon molecular sieves by templated synthesis: the structural varieties, *Stud. Surf. Sci. Catal.*, 2001, **135**, 150–157.

19 D. P. Serrano, J. A. Botas, P. Pizarro, R. Guil-López and G. Gómez, Ordered mesoporous carbons as highly active catalysts for hydrogen production by CH_4 decomposition, *Chem. Commun.*, 2008, 6585–6587.

20 Z. Bai, H. Chen, W. Li and B. Li, Hydrogen production by methane decomposition over coal char, *Int. J. Hydrogen Energy*, 2006, **31**, 899–905.

21 M. H. Kim, E. K. Lee, J. H. Jun, G. Y. Han, S. J. Kong, B. K. Lee, T.-J. Lee and K. J. Yoon, Hydrogen production by catalytic decomposition of methane over activated carbons: deactivation study, *Korean J. Chem. Eng.*, 2003, **20**, 835–839.

22 E. K. Lee, S. Y. Lee, G. Y. Han, B. K. Lee, T.-J. Lee, J. H. Jun and K. J. Yoon, Catalytic decomposition of methane over carbon blacks for CO_2-free hydrogen production, *Carbon*, 2004, **42**, 2641–2648.

23 L. Yang, X. Wu, F. Liu, X. Zhang, J. He and K. Saito, Joint-use of activated carbon and carbon black to enhance catalytic stability during chemical looping methane decomposition process, *Int. J. Hydrogen Energy*, 2020, **45**, 13245–13255.

24 D. P. Serrano, J. A. N. Botas, J. Fierro, R. Guil-López, P. Pizarro and G. Gómez, Hydrogen production by methane decomposition: origin of the catalytic activity of carbon materials, *Fuel*, 2010, **89**, 1241–1248.

25 N. Muradov, F. Smith and A. T. Raissi, Catalytic activity of carbons for methane decomposition reaction, *Catal. Today*, 2005, **102**(103), 225–233.

26 H. Teng, J. A. Ho and Y. F. Hsu, Preparation of activated carbons from bituminous coals with CO_2 activation-influence of coal oxidation, *Carbon*, 1997, **35**(2), 275–283.

27 S. Krzyzynski and M. Kozłowski, Activated carbons as catalysts for hydrogen production via methane decomposition, *Int. J. Hydrogen Energy*, 2008, **33**, 6172–6177.

28 S. Wauters and G. B. Marin, Computer generation of a network of elementary steps for coke formation during the thermal cracking of hydrocarbons, *Chem. Eng. J.*, 2001, **82**, 267–279.

29 L. Bokobza, J. L. Bruneel and M. Couzi, Raman spectroscopic investigation of carbonbased materials and their composites comparison between carbon nanotubes and carbon black, *Chem. Phys. Lett.*, 2013, **590**, 153–159.

30 S. Y. Lee, J. H. Kwak, G. Y. Han, *et al.*, Characterization of active sites for methane decomposition on carbon black through acetylene chemisorption, *Carbon*, 2008, **46**(2), 342–348.

31 S.-M. Lee, S.-H. Lee and J.-S. Roh, Analysis of Activation Process of Carbon Black Based on Structural Parameters Obtained by XRD Analysis, *Crystals*, 2021, **11**, 153.